Colchicine Reduces Lung Injury in Experimental Acute Respiratory Distress Syndrome

Jocelyn Dupuis (dupuisj@icloud.com)
Université de Montréal https://orcid.org/0000-0002-3193-1014
Martin G. Sirois
Université de Montreal
Eric Rhéaume
Université de Montréal https://orcid.org/0000-0002-0554-0984
Quang T. Nguyen
Montreal Heart Institute
Marie-Élaine Clavet-Lanthier
Montreal Heart Institute
Geneviève Brand
Montreal Heart Institute
Téodora Mihalache-Avram
Montreal Heart Institute
Gabriel Théberge-Julien
Montreal Heart Institute
Daniel Charpentier
Montreal Heart Institute
David Rhainds
Montreal Heart Institute
Paul-Éduard Neagoe
Montreal Heart Institute
Jean-Claude Tardif (Jean-Claude.Tardif@icm-mhi.org)
Montreal Heart Institute https://orcid.org/0000-0002-8200-8983

Research Article

Keywords: anti-inflammatory agents, neutrophils, therapy, lung edema, respiratory failure, flow cytometry

Posted Date: July 17th, 2020

DOI: https://doi.org/10.21203/rs.3.rs-43204/v1

Version of Record: A version of this preprint was published at PLOS ONE on December 2nd, 2020. See the published version at https://doi.org/10.1371/journal.pone.0242318.

Abstract

The acute respiratory distress syndrome (ARDS) is characterized by intense dysregulated inflammation leading to lung injury and respiratory failure. We studied the effects of colchicine pre-treatment on oleic acid-induced ARDS in rats. Colchicine reduced histological lung injury by 61%, reduced lung edema, and markedly improved blood oxygenation by increasing PaO_2/FiO_2 from 66 ± 13 mmHg (mean ± SEM) to 246 ± 45 mmHg. Lung neutrophil recruitment was reduced by colchicine with evidence for reduced neutrophils activation, as assessed by flow cytometry. This study strongly supports the clinical development of colchicine, a widely available low-cost drug, for the prevention of ARDS in conditions causing acute lung injury.

Introduction

The acute respiratory distress syndrome (ARDS) results from direct or indirect acute lung injury (ALI) leading to intense inflammation with alveolar edema producing respiratory failure. ARDS accounts for 10% of intensive care units admissions and for 24% of mechanically ventilated patients (1,2). In the United States alone, it affects approximately 200 000 patients per year with a high mortality rate ranging from 35% to 46%, higher mortality being associated with greater initial ALI (1). Furthermore, survivors of ARDS suffer from significant long-term morbidity affecting quality of life with physical, neuropsychiatric and cognitive impairments (1). Besides mechanical ventilatory support, there are no treatment options currently available and all trials with pharmacologic agents have shown neutral or even deleterious effects (3). ARDS represents the major complication of SARS-CoV-2 infection and in the context of the current COVID-19 pandemic, there is an urgent need for effective therapies that could reduce intensive care unit admissions, mechanical ventilation and death rate.

The early pathologic phase of ARDS, termed the “exudative” phase, is characterized by high-permeability alveolar edema with intense dysregulated inflammation (2,4). In this early phase following ALI, histological study reveals predominant neutrophilic alveolitis: activated polymorphonuclear neutrophils recruit to lung tissue in concert with monocytes and alveolar macrophages (5). It is recognized that neutrophils play a major role in lung tissue injury by their rapid recruitment and their release of proteases (myeloperoxidase (MPO), elastase, matrix metalloproteases (MMP), free oxygen radicals and neutrophils extracellular traps (NETs) (6,7). Initial neutrophils recruitment results from the release of pathogen-associated molecular patterns (PAMPs) and damage-associated molecular patterns (DAMPs) activating the inflammasome (6). PAMPs comprise lipopolysaccharide (LPS), lipoteichoic acid, DNA, RNA and foreign proteins such as formylated peptides released by infectious agents and recognized by immune receptors such as Toll-like receptors. DAMPs are released after tissue injury and include high mobility group box 1 (HMGB1), heat shock proteins, hyaluronan and mitochondrial-derived factors. While neutrophils play a critical role in ALI, macrophages and monocytes orchestrate resolution of inflammation and tissue repair (8) whereas CD4 regulatory T lymphocytes may play a central role in the control of neutrophil recruitment in indirect ALI (9).

Colchicine is a widely available low-cost drug proven effective in the treatment and prevention of inflammatory disorders characterized by dysregulated inflammation including gout, pericarditis and familial Mediterranean fever. More recently, colchicine prevented recurrent events after acute coronary syndrome, a disorder also characterized by inflammation with neutrophils and macrophages rich plaques (10). Colchicine inhibits tubulin polymerization in leukocytes reducing their adhesion, recruitment and activation. Colchicine abrogated NETs formation in acute coronary syndrome patients after percutaneous coronary intervention (11) and in patients with active Behçet's disease (12). It also reduces inflammation by interfering with leukocytes inflammasome activation, in particular the NLRP3 complex (13,14) and therefore may lead to decreased levels of proinflammatory cytokines 1L-1b and IL-6 (15).

The COLCORONA trial is an international randomized double-blind placebo-controlled study of 6 000 patients currently evaluating colchicine for the prevention of COVID-19-related complications. In that context, we evaluated if colchicine pre-treatment could reduce ALI, inflammation and respiratory failure in a well characterized model of ARDS. Rats were pre-treated with colchicine (1mg/kg/day) or placebo for 3 days prior to oleic acid-induced ALI and compared to a control group 4 hours after ALI.

Results

Effects of colchicine on lung edema and gas exchanges (Figure 1). Oleic acid induced severe ALI with almost tripling of lung weight and severe edema evidenced by increased wet/dry lung weight ratio. Macroscopically, the lungs were larger and hemorrhagic. There was severe respiratory failure with markedly reduced blood oxygenation. The animals were administered 100% FiO_2 before arterial blood gas sampling so that the measured PaO_2 is equivalent to the PaO_2/FiO_2, a recognized parameter indicative of ARDS severity. Clinical ARDS is recognized when the PaO_2/FiO_2 is less than 300. Oleic acid caused severe respiratory failure as the PaO_2 decreased from 380 ± 18 mmHg to 66 ± 13 mmHg (mean ± SEM) with CO_2 retention causing respiratory acidosis. Colchicine therapy reduced pulmonary edema, markedly improved blood oxygenation with a PaO_2 of 246 ± 45 mmHg and reduced respiratory acidosis.

Effects of colchicine on respiratory parameters, blood cell counts and biochemistry (Table 1). Animals with oleic acid injury had increased respiratory rate with lower tidal volume. Both were improved although non-significantly with colchicine therapy. Oleic acid injection caused an increase in blood hemoglobin and hematocrit, the latter being statistically significant. Colchicine therapy normalized both hemoglobin and hematocrit, the latter being no longer significantly different from those of the sham animals. Oleic acid increased leukocyte count, the increase being statistically significant in the colchicine treated animals compared to the sham group. This increase was mostly caused by an elevation in neutrophils, also significant in the colchicine treated animals only. There was a mild non-significant increase in lymphocytes after oleic acid, with no effect of colchicine therapy. Platelet count was significantly reduced by oleic acid injury, and partly normalized after colchicine therapy, being no-longer different from the sham group. Oleic acid caused a marked elevation of plasma glucose that was significantly reduced by

colchicine therapy. Inversely, plasma natremia was reduced by oleic acid and improved by colchicine. There was no difference on corrected calcium, lactates and bicarbonates between groups.

Effects of colchicine on lung injury, neutrophil recruitment and NETs formation (Figure 2). All samples were analyzed by a technician blinded to treatment assignment. Oleic acid caused important histological lung injury. Representative examples of the appearance of the complete left lung at low magnification demonstrates evident zones of severe damage, markedly reduced in colchicine-treated animals. The proportion of injured area in the oleic acid ALI group was 24.6 ± 2.4% with a 61% relative reduction down to 9.6 ± 3.1% after colchicine treatment. The lung injury score (maximum score of 70) was markedly elevated after oleic acid from 5.1 ± 0.8 in sham to 44 ± 2.8, and markedly reduced by colchicine to 28.7 ± 5.0. Mean alveolar wall thickness more than doubled after oleic acid from 4.6 ± 0.3 µm to 10.9 ± 1.1 µm and this was also significantly reduced by colchicine to 7.8 ± 1.1 µm. Both the lung injury score and alveolar wall thickness were inversely correlated with the severity of ARDS measured from the PaO_2. Lung neutrophil recruitment, as assessed by MPO immunostaining, was greatly increased after ALI from 1.16 ± 0.19% to 8.86 ± 0.66% and significantly reduced by colchicine therapy to 5.95 ± 1.13%. Lung neutrophils undergoing NETosis were assessed by measuring citrullinated histone H3 (Cit-H3) immunostaining intensity. Treatment with oleic acid increased basal NETosis by 63%, whereas colchicine therapy nearly halved the induction of NETosis, bringing it back to a 35% increase over basal level, a value no longer statistically different from the control group.

Effects of colchicine on circulating cytokines (supplemental Figure 1). Oleic acid-induced ALI was associated with an increase in mean serum IL-6, TNF-α and KC/GRO. There was a trend towards reduced IL-6 level with colchicine, and TNF-α and KC/GRO were also non-significantly reduced by therapy. There was no change in any of the other cytokines measured: Cit-H3, INF-g, IL-10, IL-13, IL-4 and IL-5. IL-1â level was too low to be quantified in 14 of the 20 rats.

Effects of colchicine on blood leukocyte activation evaluated by flow cytometry (Figure 3). Leukocyte count on flow cytometry demonstrated an increase in neutrophils that was significant in colchicine treated animals, but no change in lymphocytes counts. A leukocyte activation assay was performed on rat blood samples obtained at the time of sacrifice by in vitro LPS stimulation (500 ng/mL) and analysis of the surface expression of CD11b, a member of the β2 integrin family. In sham-treated rats, LPS stimulation resulted in approximately a 2-fold increase of cell surface CD11b mean fluorescence intensity (MFI). Oleic acid exposure tended to decrease the response to LPS in leukocytes and significantly reduced the response in granulocytes, whereas colchicine restored the normal response to LPS stimulation. In unstimulated blood from oleic acid treated animals, we observed an increase in His48 fluorescence of neutrophils that was normalized by colchicine treatment. Additionally, cell surface CD4 and CD8 on respective lymphocyte sub-populations were increased after oleic acid stimulation, and also normalized by colchicine therapy.

Effects of colchicine on markers of inflammation and injury in lung tissue (Figure 4). The mRNA expression of 27 genes involved in inflammatory responses and injury was measured in lung tissue. The

results, summarized in a clustered heatmap, clearly demonstrate lung tissue transcriptional regulation of these genes in oleic acid-exposed rats. There was, however, no individual statistically significant effect of colchicine therapy.

Discussion

Acute direct or indirect lung injury leading to ARDS represents a serious critical care condition with no effective pharmacologic treatment option (2). We used the oleic acid model of ARDS to evaluate the effects of colchicine on the acute exudative inflammatory phase of this condition. Colchicine pre-treatment for three days effectively reduced lung edema and markedly improved gas exchanges with increased blood oxygenation and reduced respiratory acidosis. Colchicine reduced ALI evidenced by a reduction in the injured area of 61%, a reduction of the lung injury score in affected regions and reduced alveolar wall thickness correlating with the improved gas exchange. The benefit of colchicine therapy was related to a reduction in lung recruitment and activation of neutrophils.

Relevance of this animal model to SARS- CoV-2 respiratory failure. Oleic acid (18:1 n-9), an unsaturated long-chain fatty acid, is the most abundant fatty acid in nature and in the human body. Oleic acid in physiologic concentrations is bound to plasma albumin and non-toxic. Human subjects who develop ARDS have higher plasma levels of C18 unsaturated fatty acids (16). Injection of high concentrations of oleic acid causes rapid high permeability lung edema with inflammation and impaired gas exchanges and mechanics (17) reproducing human ARDS. Lung injury occurs rapidly after less than 5 minutes (18) with neutrophils infiltration and production of cytokines and chemokines (17). The acute lung damage caused by oleic acid is characterized by important neutrophils accumulation and activation leading to intense inflammation (17), concordant with the pathophysiology of human ARDS (2). Besides direct injury through lung embolization, oleic acid stimulates free fatty acid receptors-1 and GPR120 and activates numerous intracellular pathways of inflammation (17).

Shared similarities between the oleic acid model of ARDS and coronavirus induced ARDS are the immune dysregulation with intense inflammation associated with lung neutrophil recruitment as well as cytokines elevations. These were well described for the SARS-CoV-1 and MERS-CoV infections (19). Among the potential inflammatory pathways shared by oleic acid toxicity and coronaviruses is the NLRP3 inflammasome pathway. This cytoplasmic pattern recognition receptor is present in neutrophils and is activated in the lungs after oleic acid injury (20). It has been shown that activation of NLRP3 by SARS-CoV is a mechanism triggering the inflammatory response to this infection (21). Although not specifically addressed in this study, colchicine inhibits the NLRP3 inflammasome pathway (14) and this could therefore represent a mechanism of benefit in this model. The numerical reduction in plasma concentration of IL-6 with colchicine observed in the current study is in line with an effect on the inflammasome.

Mechanisms of colchicine benefit. As previously described, oleic acid injection caused circulating leukocytosis predominantly involving neutrophils and important lung recruitment of neutrophils.

Colchicine therapy did not reduce circulating neutrophilia, but nevertheless markedly reduced lung recruitment of neutrophils as assessed from MPO immunostaining. Release of neutrophils elastase, myeloperoxydase and NETs contribute to ALI leading to pulmonary edema, alveolar wall thickening and altered gas exchanges with reduced PaO_2 and increased $PaCO_2$. Following the reduction in lung neutrophils recruitment, all of these parameters were improved by colchicine therapy. The lack of effect of colchicine on increased circulating neutrophils suggests that treatment did not interfere with early signaling events responsible for bone marrow release of neutrophils. In addition, it is possible that colchicine caused less neutrophils adhesion to microvasculature and/or transvascular emigration, as observed in lungs, and this might have contributed to the higher neutrophil cell count in circulating blood. Our flow-cytometry analysis on whole blood from these animals however demonstrates that colchicine modified the biology of oleic acid-treated neutrophils and “normalized” their response to LPS and reduced the expression the His48 antigen. A previous study in a very inflammatory model of *Pneumocystis* pneumonia demonstrated an accumulation of $CD11bc^+$ and $His48^+$ cells in the lungs identified as myeloid-derived suppressor cells (22). Transfer of these cells, which morphologically resemble neutrophils, to control mice caused acute lung damage (22). Reduction of neutrophil’s His48 expression by colchicine treatment may therefore be associated with less “primed” or less damaging neutrophils and provide protection against lung injury. Oleic acid injury was associated with an increase in the plasma cytokines IL-6, TNF-α and KC/GRO (CXCL-1) that was reduced, although non-significantly, by colchicine. Together, these data support that colchicine reduced neutrophils activation with reduced lung recruitment in response to oleic acid injury.

We measured lung tissue mRNA expression of 27 selected markers of lung injury and inflammation. A clustered analysis reveals strong differential activation after oleic acid injury. There was however no statistically significant effect of colchicine on these individual parameters. We believe that this may be in part due to the heterogeneous nature of ALI in the model as evidenced in Figure 2, where damaged zones are interspaced by healthier zones. Analysis of lung tissue homogenates may “dilute” the effect of therapy by including healthier zones into the samples. Selected sampling of injured zones by microdissection may be required to detect treatment effects on these different pathways. Sampling time after injury may also explain the findings as we limited our evaluation at 4 hours and longer duration may be necessary to detect transcriptomic benefits of colchicine treatment. Finally, our sample size may be underpowered to detect a statistically significant difference in these parameters that may have been differently affected in individual animals.

Variability in the response to colchicine and effect in other ALI models. Although oleic acid caused similar level of injury in animals, we observed individual variability in the benefit of colchicine therapy on lung edema and blood oxygenation. Since Wistar rats are an outbred strain, genetic variability may account for variable benefits of therapy. Also, previous investigations have shown the importance of individual metabolomic profiles of same strain laboratory animals, dependent on environment and microbiota, on the variable response to pharmacologic intervention (23). In subjects with familial Mediterranean fever,

small intestine bacterial overgrowth has been associated with reduced response to colchicine therapy (24).

Other studies have evaluated the effect of colchicine in animal models of ARDS and found similarly beneficial effects. In a mouse model of ALI induced by inhalation of the toxic gas phosgene, colchicine reduced lung neutrophil recruitment, lung injury and mortality (25). The benefit was seen even with colchicine administration 30 minutes after phosgene exposure. In yet another different model of ALI caused by hyperoxia in rat pups, colchicine reduced lung injury and lowered TNF-α and IL-1β levels in broncho-alveolar lavage fluids (26). Together with the current study, these data support the effectiveness of colchicine for the treatment of ALI of various etiologies.

Limitations and perspective. The results of the current pre-clinical study of ARDS cannot be extrapolated to human ARDS, but strongly support the conduct of properly sized randomized clinical trials. The Colchicine Coronavirus SARS-CoV2 Trial (COLCORONA, NCT04322682) is currently recruiting 6 000 subjects with SARS-CoV-2 infection to colchicine treatment or placebo to reduce hospitalizations and deaths. This international trial is the largest clinical COVID-19 related trial currently underway. Since dysregulated immunity plays a major role in ARDS due to COVID-19 and because of the low cost and wide availability of colchicine, our results strongly support recruitment efforts into this trial.

Conclusion

Colchicine pre-treatment reduces ALI and lung edema and markedly improves blood oxygenation in the oleic acid model of ARDS by reducing lung neutrophil recruitment and activation. These results strongly support the re-purposing of colchicine, a low cost and widely available drug, in trials of human ARDS.

Methods

The study protocol was approved by the animal research and ethics committees of the Montreal Heart Institute and all experiments conducted in accordance with the Canadian guidelines for the care of laboratory animals.

Animal model and colchicine administration. Male Wistar rats weighing 250–300 g were purchased from Charles River, St. Constant, Québec. They were divided in three groups: Sham + placebo (n=8), oleic acid + placebo (n=8) and oleic acid + colchicine (n=8). Oleic acid (150 mg/kg in 0.3 cc) was prepared daily as a mixture with 0.1% bovine serum albumin (BSA) dissolved in distilled water, stored and protected from light at room temperature. Colchicine (1mg/kg) or distilled water (placebo) was administered by daily gavage (in a volume up to 2 ml/kg) for three days before the induction of the ALI model. On the beginning of the fourth day a last forth dose of colchicine or placebo was administered and rats immediately injected via a jugular vein cannula with oleic acid or with 0.1% BSA. There was no death in the sham group. There was one death in the oleic acid + placebo group 3 hours after injection of oleic acid and

prior to any measurement. There was one surgical death in oleic acid + colchicine treatment by laceration of the jugular vein, prior to injection of oleic acid.

Oleic acid was administered under ketamine/xylazine anesthesia by slow bolus injection over 30 seconds and the catheter was flushed with 0.3 ml of 0.1% BSA before and after injection. Four hours later, the animals were studied. Conscious unrestrained respiratory parameters were obtained by whole body plethysmography (Emka technologies). Rats were then anesthetized with 2.5% isoflurance and 100% oxygen (1L/min) administered with a nose cone/face mask for a duration of 5 minutes before terminal exsanguination. 2ml of arterial blood was collected through the thoracic aorta into a syringe containing lyophilized heparin for arterial blood gas assessment. The remaining of blood was collected into EDTA Lavendar tubes for complete blood count and flow cytometry. Cytokines measurements were assessed with serum isolated with serum clot activator tubes.

The lungs were excised for analysis: the left lung was cannulated and perfusion-fixed with 10% buffered formalin for histology and immunohistochemistry. The right superior and middle lobes were used to measure the lung weight and edema. The inferior lobes of the right lung were snap-frozen and stored at -80 °C for gene expression analysis. Pulmonary edema was measured from the ratio of total divided by dry weight of the right lung. Total weight, including water, was measured and lung tissue was dried in an oven at 60 °C for 5 days and reweighted as dry weight.

Lung histology and immunohistology. All histological and immunohistological procedures were performed by the same person blinded to treatment assignment. The left lung was cannulated and perfused with 10% formalin PBS-buffered solution and fixed for 5 days. Tissues were dehydrated by incubating in a series of solutions with an increased ethanol content (70, 95 and 100%), followed by xylene, and embedded in paraffin. The specimens were cut into 6-µm sections, mounted on charged slides and processed with hematoxylin phloxine saffron (HPS) staining.

Immunohistological procedures were initiated by incubating the slides in citrate antigen retrieval (pH 6.0) and endogenous peroxidase blocking (3% hydrogen peroxide). Sections were then blocked by incubating in PBS containing 10% normal goat serum (same species as secondary antibody) for 60 minutes. Slides were incubated with a rabbit polyclonal anti-myeloperoxidase (MPO, Pa5-16672; ThermoFisher, MA USA) for neutrophil detection, with a rabbit polyclonal anti-histone H3 citrulline R2 + R8 + R17, (Cit-H3, ab5103; ABCAM, Cambridge, United Kingdom) for NETosis and primary antibodies were omitted for negative controls. After washing, sections were incubated with a biotinylated secondary antibody (Vector Laboratories, Burlingame, CA) for 30 minutes, washed, then incubated with avidin-biotin complex (ABC kit) and visualized using diaminobenzidine substrate (Vector Laboratories) (27-29).

The HPS slides were scanned to get a picture of the whole left lung (Super coolscan 5000; Nikon, Tokyo Japan). Using a brightfield microscope (BX45, Olympus, Richmond Hill, ON, Canada), images were acquired under 200× magnification on the most damaged/altered regions, acquiring 5 fields per slide for the HPS staining and 10 fields per slide for IHC (MPO and Cit-H3) staining. For the HPS staining, the

following analyses were performed: 1) thickness of alveolar membranes, 2) percentage (%) of altered lung tissue, 3) injury score of the lungs.

To assess the thickness of alveolar membranes, 20 measurements per field were performed (corresponding to 100 measurements per slide) and were expressed as the mean thickness (µm) of the alveolar membranes. A morphometric analysis has been performed to assess the percentage of altered lung tissue over total lung area (excluding trachea, major bronchi and blood vessels >700 µm diameter). To evaluate lung injury, we used an adapted version of the standardized histology score from the American Thoracic Society Documents (30). The histology scores (0, 1 or 2), were given for: 1) neutrophils in the alveolar space, 2) neutrophils in the interstitial space, 3) proteinaceous debris, 4) alveolar septal thickening, 5) alveolar hemorrhage, 6) interstitial space/membrane hemorrhage and 7) alveolar necrosis. For each slide the maximal injury score, corresponding to the sum of the score (score 0 to 2) of the 7 parameters x 5 fields per slide, is 70 points (2x7x5).

Neutrophils immunoreactivity in the lungs was performed to assess the presence of neutrophils (MPO immunostaining) and neutrophils undergoing NETosis (Cit-H3). The percent area (%) occupied by neutrophils in the lungs was quantified by color segmentation and represented as the MPO area over total lung tissue area. To assess neutrophils undergoing NETosis, we quantified the intensity of Cit-H3 staining (lumen). All analyses were performed using Image Pro Premier version 3.0 software (Media Cybernetics, Rockville, MD, USA).

Serum cytokine quantification. Quantitative determination of serum IFN-γ, IL-1β, IL-4, IL-5, IL-6, KC/GRO, IL-10, IL-13, and TNF-α was done using the electrochemiluminescence-based Meso Scale Discovery (MSD) platform (Rockville, Maryland, USA). Proteins levels were measured in a multiplex assay using the V-PLEX Proinflammatory Panel 2 Rat kit (MSD). Samples were diluted 1:5 in proprietary buffer (MSD) and measured. Data were acquired using a MESO QuickPlex SQ 120 plate reader (MSD) and protein concentrations were determined using the MSD Discovery Workbench 4.0 analysis software. All values reported are between the lower and the upper limits of quantification of the kit. Quantitative determination of serum Cit-H3 was measured by a commercially available ELISA kit (Cayman Chemical, 501620, Ann Arbor, MI, USA).

Flow cytometry

In vitro **LPS challenge of blood leukocytes**. Whole blood samples collected on EDTA-coated tubes were incubated or not with LPS (500 ng/mL) for 30 minutes at 37°C. The samples were then stained using mouse anti-rat CD45 Alexa Fluor 700 (clone OX-1, conjugated to Alexa Fluor 700, Biolegend), mouse anti-rat CD11b antibody (clone WT.5, conjugated to V450, BD Horizon) and 7AAD (Biolegend) for 30 minutes at 4°C. FACS lysing solution (BD Pharm Lyse, BD Biosciences) was added for 15 minutes at room temperature and samples were stored at 4°C until analysis by flow cytometry (LSRII, BD Biosciences). Data were analyzed on Diva software version 8.0.1 (BD Biosciences).

Leukocyte immunophenotyping. Using reverse pipetting, 100 µl of whole blood collected on EDTA-coated tubes were incubated with anti-CD32 to prevent FC-mediated non-specific binding according to the manufacturer's instructions. The panel of antibodies as well as the gating strategy were inspired by Barnett-Vanes and al. (31). Briefly, a panel of 11 antibodies (Supplemental Table 1) was used to identify the neutrophils ($CD45^+$/ SSChi / $His48^+$), the monocytes ($CD45^+$/ SSC^{lo}/ $His48^{hi\ or\ lo}$/$CD43^{hi\ or\ lo}$), the B lymphocytes ($CD45^+$/ SSC^{lo} /$CD45R^-B220^+$), the T lymphocytes ($CD45^+$/ SSC^{lo} / $CD3^+$/$CD4^+$ or $CD8^+$) and the natural killer cells ($CD45^+$/SSC^{lo} /$CD161a^+$). The whole blood samples were incubated with the antibodies for 20 minutes at room temperature and the BD Pharm Lyse solution was then added for 10 minutes to lyse the erythrocytes. Samples were stored at 4°C until analysis by flow cytometry (LSRII BD Biosciences). Accucount (Spherotech) were added to establish a cell count per µl of blood. Data were analyzed on Diva software version 8.0.1 (BD Biosciences).

RNA extraction and quantification of mRNA expression by RT-qPCR analysis

Tissue homogenization, RNA extraction, RT-PCR and real-time PCR. About 30 mg of rat lung samples were homogenized in a TissueLyser II (Qiagen, Germany) in 700 µL of RLT buffer from the RNeasy Mini RNA extraction kit (Qiagen, Germany) supplemented with the anti-foam DX Reagent. Total RNA was-extracted according to the kit's instructions. RNA integrity and quantity were assessed using a 2100 Bioanalyzer Instrument (Agilent, Santa Clara, CA). 500 ng of RNA were used for cDNA synthesis using the High-Capacity cDNA Reverse Transcription Kit (Applied Biosystems, Foster City, CA). For RT-qPCR, reactions were performed in duplicates using the SsoAdvanced Universal SYBR Green Supermix (Bio-Rad, Hercules, CA), 2.5 ng of cDNA and a final concentration of 100 nM of each primer. The cycling protocol started with a denaturation step at 95°C for 5 min, followed by 40 cycles of denaturation at 95°C for 15 s and primer annealing and extension at 57°C for 30 sec. Upon completion of the cycling steps, a melting curve protocol was performed from 60°C to 95°C and the reaction was stored at 4°C. Real-time PCR was carried out using a CFX384 Touch Real-Time PCR Detection System (Bio-Rad, Hercules, CA). The geometric mean of housekeeping genes ACTB, GAPDH and XBP1 was used as an internal control to normalize the variability in expression levels which were analyzed using the $2^{-\Delta\Delta CT}$ method. The primer sequences are provided in Supplemental Table 2. Heat maps of normalized expression values for gene expression was generated using Morpheus from Broad Institute (https://software.broadinstitute.org/morpheus). To normalize the data, the $\log_2$ of normalized expression values for IL-2, IL-13, CXCR2, E-sel, Arg1, CXCL1, CalCRL, Ramp2 and ATP1B1 were used.

Statistical analysis. Comparisons between groups were performed by one-way ANOVA followed by Tukey's post-hoc comparisons. Significant differences were considered if $p<0.05$. All values are presented as mean ± SEM.

Declarations

Acknowledgements. This study was funded by the Government of Quebec and the Canada Research Chair in translational and personalized medicine held by Dr. Tardif.

Competing interests. The authors declare no competing interests.

References

1. Bellani G, Laffey JG, Pham T et al. Epidemiology, patterns of care, and mortality for patients with acute respiratory distress syndrome in intensive care units in 50 countries. JAMA 2016;315:788-800.
2. Thompson BT, Chambers RC, Liu KD. Acute respiratory distress syndrome. N Engl J Med 2017;377:1904-1905.
3. Fan E, Brodie D, Slutsky AS. Acute respiratory distress syndrome: Advances in Diagnosis and Treatment. JAMA 2018;319:698-710.
4. Sweeney RM, McAuley DF. Acute respiratory distress syndrome. Lancet 2016;388:2416-2430.
5. Wong JJM, Leong JY, Lee JH, Albani S, Yeo JG. Insights into the immuno-pathogenesis of acute respiratory distress syndrome. Ann Transl Med 2019;7:504.
6. Prame Kumar K, Nicholls AJ, Wong CHY. Partners in crime: neutrophils and monocytes/macrophages in inflammation and disease. Cell Tissue Res 2018;371:551-565.
7. Potey PM, Rossi AG, Lucas CD, Dorward DA. Neutrophils in the initiation and resolution of acute pulmonary inflammation: understanding biological function and therapeutic potential. J Pathol 2019;247:672-685.
8. Herold S, Mayer K, Lohmeyer J. Acute lung injury: how macrophages orchestrate resolution of inflammation and tissue repair. Front Immunol 2011;2:65.
9. Venet F, Chung CS, Huang X, Lomas-Neira J, Chen Y, Ayala A. Lymphocytes in the development of lung inflammation: a role for regulatory CD4+ T cells in indirect pulmonary lung injury. J Immunol 2009;183:3472-80.
10. Tardif JC, Kouz S, Waters DD et al. Efficacy and safety of low-dose colchicine after myocardial infarction. N Engl J Med 2019;381:2497-2505.
11. Safı R, Kallas R, Bardawil T et al. Neutrophils contribute to vasculitis by increased release of neutrophil extracellular traps in Behcet's disease. J Dermatol Sci 2018;92:143-150.
12. Vaidya K, Tucker B, Kurup R et al. Colchicine inhibits neutrophil extracellular trap formation in acute coronary syndrome patients after percutaneous coronary intervention. medRxiv 2020:2020.04.20.20034025.
13. Otani K, Watanabe T, Shimada S et al. Colchicine prevents NSAID-induced small intestinal injury by inhibiting activation of the NLRP3 inflammasome. Sci Rep 2016;6:32587.
14. Martinez GJ, Celermajer DS, Patel S. The NLRP3 inflammasome and the emerging role of colchicine to inhibit atherosclerosis-associated inflammation. Atherosclerosis 2018;269:262-271.
15. Martinez GJ, Robertson S, Barraclough J et al. Colchicine acutely suppresses local cardiac production of inflammatory cytokines in patients with an acute coronary syndrome. J Am Heart Assoc 2015;4:e002128.

16. Bursten SL, Federighi DA, Parsons P et al. An increase in serum C18 unsaturated free fatty acids as a predictor of the development of acute respiratory distress syndrome. Crit Care Med 1996;24:1129-36.
17. Goncalves-de-Albuquerque CF, Silva AR, Burth P, Castro-Faria MV, Castro-Faria-Neto HC. Acute respiratory distress syndrome: role of oleic acid-triggered lung injury and inflammation. mediators inflamm 2015;2015:260465.
18. Beilman G. Pathogenesis of oleic acid-induced lung injury in the rat: distribution of oleic acid during injury and early endothelial cell changes. Lipids 1995;30:817-23.
19. Channappanavar R, Perlman S. Pathogenic human coronavirus infections: causes and consequences of cytokine storm and immunopathology. Semin Immunopathol 2017;39:529-539.
20. Chen H, Ding Y, Chen W, Feng Y, Shi G. Glibenclamide alleviates inflammation in oleic acid model of acute lung injury through NLRP3 inflammasome signaling pathway. Drug Des Devel Ther 2019;13:1545-1554.
21. Chen IY, Moriyama M, Chang MF, Ichinohe T. Severe Acute Respiratory Syndrome Coronavirus Viroporin 3a Activates the NLRP3 Inflammasome. Front Microbiol 2019;10:50.
22. Zhang C, Lei GS, Shao S, Jung HW, Durant PJ, Lee CH. Accumulation of myeloid-derived suppressor cells in the lungs during Pneumocystis pneumonia. Infect Immun 2012;80:3634-41.
23. Li H, Ni Y, Su M et al. Pharmacometabonomic phenotyping reveals different responses to xenobiotic intervention in rats. J Proteome Res 2007;6:1364-70.
24. Verrecchia E, Sicignano LL, La Regina M et al. Small intestinal bacterial overgrowth affects the responsiveness to colchicine in familial mediterranean fever. Mediators Inflamm 2017;2017:7461426.
25. Ghio AJ, Kennedy TP, Hatch GE, Tepper JS. Reduction of neutrophil influx diminishes lung injury and mortality following phosgene inhalation. J Appl Physiol (1985) 1991;71:657-65.
26. Ozdemir R, Yurttutan S, Talim B et al. Colchicine protects against hyperoxic lung injury in neonatal rats. Neonatology 2012;102:265-9.
27. Perdomo J, Leung HHL, Ahmadi Z et al. Neutrophil activation and NETosis are the major drivers of thrombosis in heparin-induced thrombocytopenia. Nat Commun 2019;10:1322.
28. Nawaito SA, Sahadevan P, Clavet-Lanthier ME et al. MK5 haplodeficiency decreases collagen deposition and scar size during post-myocardial infarction wound repair. Am J Physiol Heart Circ Physiol 2019;316:H1281-H1296.
29. Sinnathamby T, Yun J, Clavet-Lanthier ME, Cheong C, Sirois MG. VEGF and angiopoietins promote inflammatory cell recruitment and mature blood vessel formation in murine sponge/Matrigel model. J Cell Biochem 2015;116:45-57.
30. Matute-Bello G, Downey G, Moore BB et al. An official American Thoracic Society workshop report: features and measurements of experimental acute lung injury in animals. Am J Respir Cell Mol Biol 2011;44:725-38.

31. Barnett-Vanes A, Sharrock A, Birrell MA, Rankin S. A single 9-colour flow cytometric method to characterise major leukocyte populations in the rat: validation in a model of LPS-induced pulmonary inflammation. PLoS One 2016;11:e0142520.

Tables

Table 1. Effect of colchicine on respiratory parameters, blood cell counts and biochemistry

	Sham	OA control	OA + colchicine
Breathing rate (bpm)	102 ± 6	181 ± 10***	166 ± 20**
Tidal volume (ml)	2.67 ± 0.15	1.19 ± 0.05***	1.81 ± 0.35*
Peek inspiratory flow (ml/s)	16.01 ± 1.23	16.43 ± 0.80	17.75 ± 2.72
Peek expiratory flow	15.48 ± 1.16	11.83 ± 0.68	13.19 ± 1.41
Hemoglobin (g/L)	150 ± 2	158 ± 3	153 ± 2
Hematocrit (%)	45.0 ± 0.6	48.7 ± 0.8**	46.6 ± 0.5
Leukocytes (10^9/L)	2.32 ± 0.29	3.75 ± 0.49	4.90 ± 0.68**
Platelets (10^9/L)	1029 ± 15	844 ± 57*	986 ± 56
Neutrophils (10^9/L)	1.14 ± 0.17	2.00 ± 0.35	2.71 ± 0.36**
Lymphocytes (10^9/L)	1.31 ± 0.15	1.77 ± 0.18	2.19 ± 0.33
Glucose (mmol/L)	16.8 ± 1.3	27.0 ± 0.6****	21.7 ± 1.6*, ††
Sodium (mmol/L)	143.7 ± 0.7	138.3 ± 0.9***	141.4 ± 0.9†
Calcium (mmol/L)[1]	1.38 ± 0.01	1.42 ± 0.01	1.40 ± 0.01
Lactate (mmol/L)	2.31 ± 0.26	1.90 ± 0.37	2.4 ± 0.53
Bicarbonate (mmol/L)	26.0 ± 0.7	28.1 ± 1.1	27.6 ± 0.8

*, **, ***, **** is for p <0.05, 0.01, 0.001, 0.0001 versus Sham respectively. †,†† is for p <0.05, 0.01 versus OA+Placebo respectively.

All values are mean ± SEM. [1]Calcium corrected for pH.

Figures

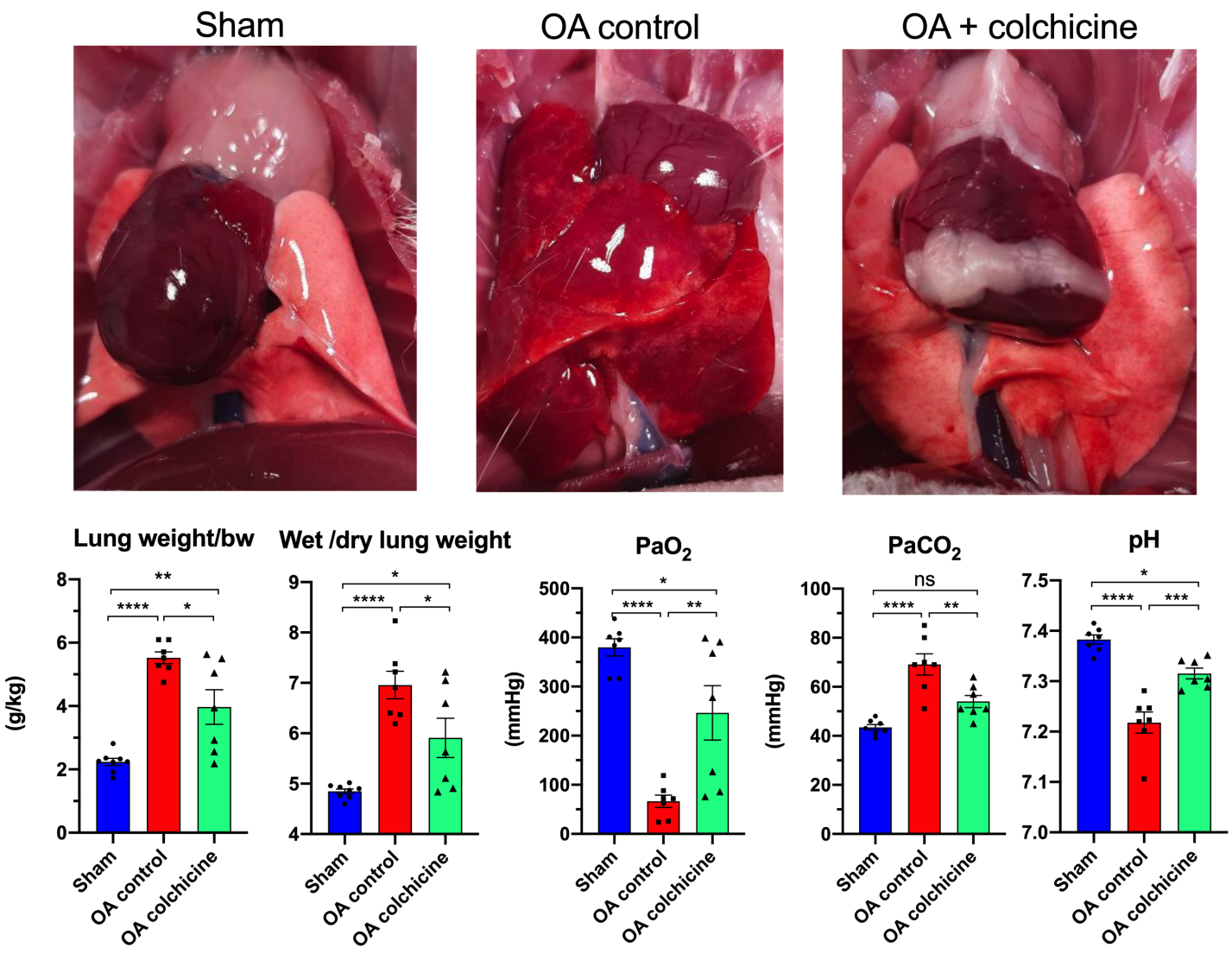

**** p<0.0001; *** p<0.001, ** p<0.01; * p<0.05

Figure 1

Effects of colchicine therapy on oleic acid-induced ALI, lung edema and gas exchange. Values are mean ± SEM. **** p<0.0001; *** p<0.001, ** p<0.01; * p<0.05.

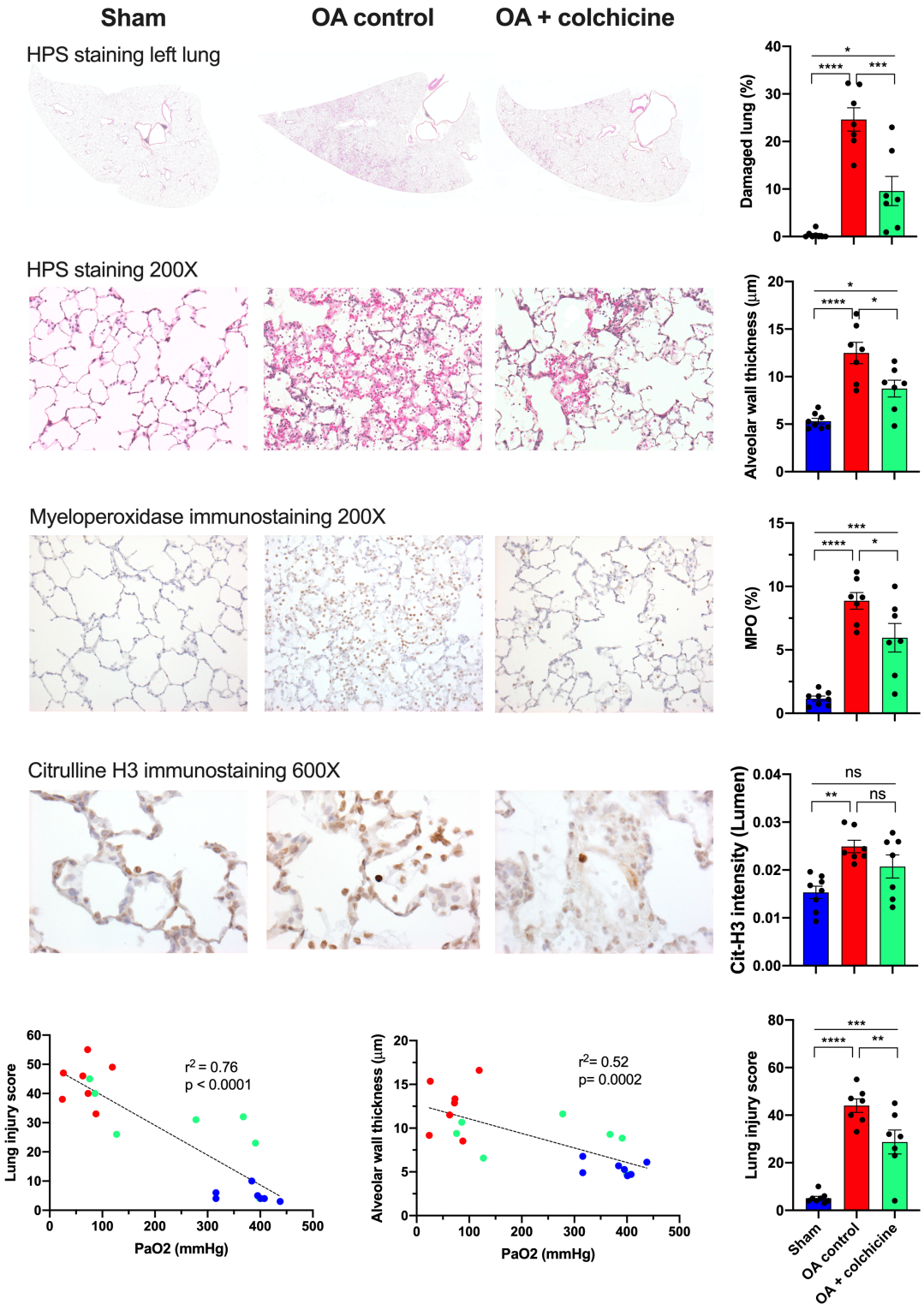

Figure 2

Effects of colchicine therapy on lung injury, neutrophils recruitment and NETosis after oleic acid-induced ALI. Values are mean ± SEM. **** p<0.0001; *** p<0.001, ** p<0.01; * p<0.05.

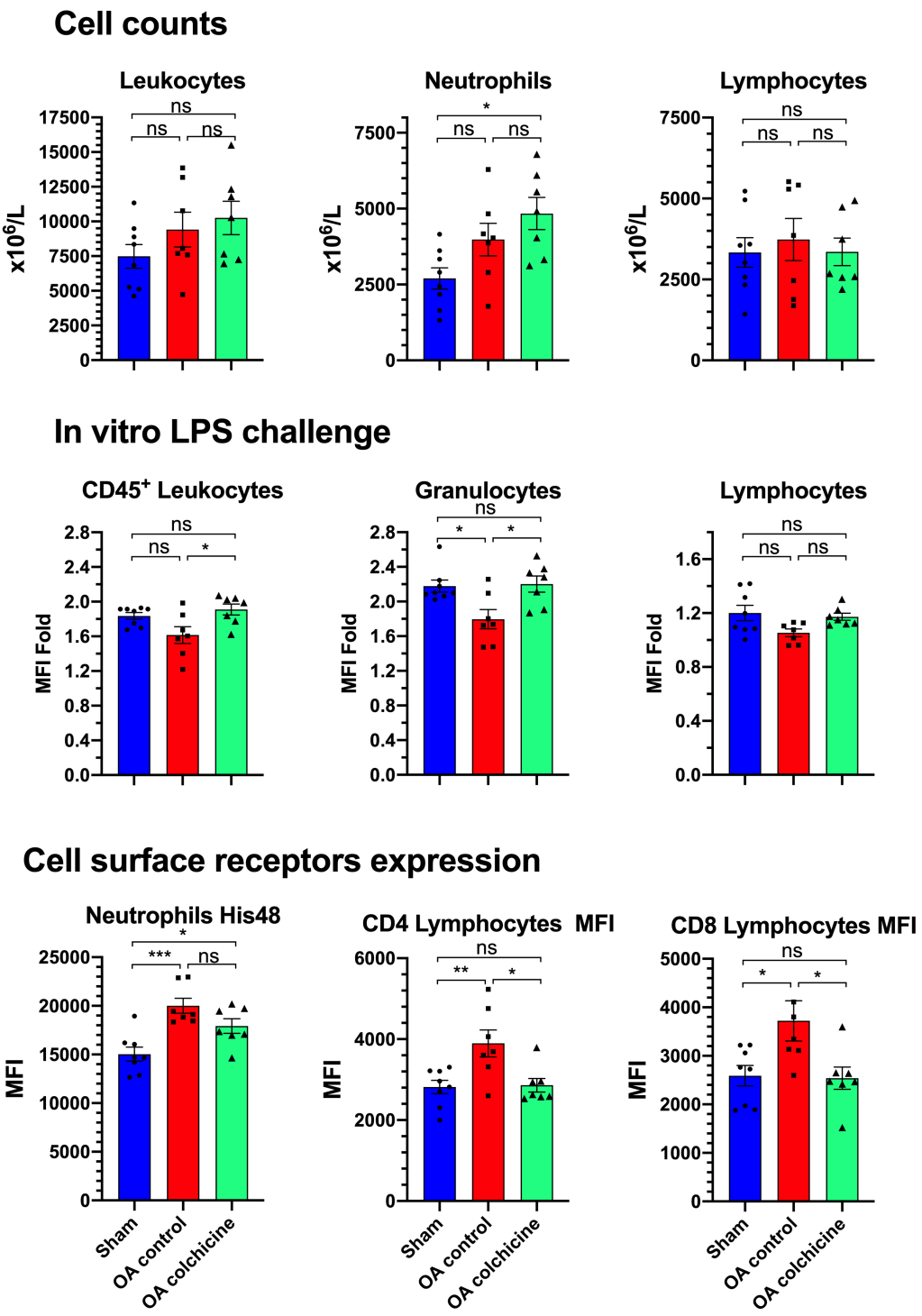

Figure 3

Whole blood flow cytometry analysis of leukocytes after oleic acid-induced ALI and effects of colchicine therapy. MFI, mean fluorescence intensity. Values are mean ± SEM. *** p<0.001, ** p<0.01; * p<0.05.

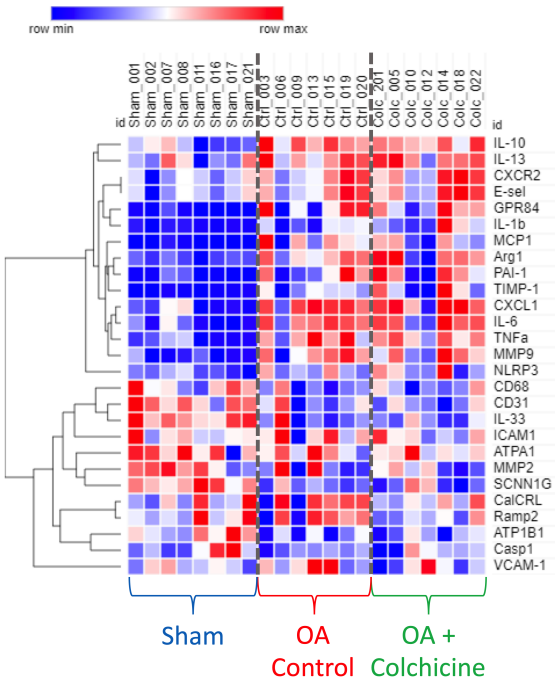

Figure 4

Clustered heatmap representation of unsupervised clustering of lung tissue mRNA expression of 27 selected markers of inflammation and injury.

Supplementary Files

This is a list of supplementary files associated with this preprint. Click to download.

- supplfig1.tiff
- SupplementalTables.docx